Available online at www.sciencedirect.com
SCIENCE DIRECT
International Journal of Mass Spectrometry 254 (2006) 44–52
International Journal of Mass Spectrometry
www.elsevier.com/locate/ijms

Memory effect in deuterium analysis by continuous flow isotope ratio measurement

Jesper Olsen [a,*], Inger Seierstad [b], Bo Vinther [b], Sigfús Johnsen [b], Jan Heinemeier [a]

[a] *Department of Physics and Astronomy, Aarhus University, Ny Munkegade bygning 520, DK-8000 Aarhus C., Denmark*
[b] *Niels Bohr Institute for Astronomy, Physics and Geophysics, Juliane Mariesvej 30, DK-2100 Copenhagen Ø, Denmark*

Received 30 December 2005; received in revised form 4 May 2006; accepted 5 May 2006
Available online 27 June 2006

Abstract

The method of deuterium analysis (δ*D*) measurements has previously been shown to suffer from intersample memory effects. In this study the memory effect of δ*D* continuous flow isotope ratio mass spectrometry (CF-IRMS) employing the chromium reduction technique is investigated with the goal of optimising the system configuration. By optimising the system configuration, the magnitude of the memory effect has been reduced from 6% to 1–2%. It is shown that the memory effect displays a long range behaviour which can be described by a sum of two exponential decay functions, indicating two main sources with different time constants. Furthermore, a correction algorithm which takes into account the observed long range nature of the memory effect is developed and tested against waters of known isotopic composition.

Keywords: δ*D* deuterium measurements; CF-IRMS; Memory effect; Correction

1. Introduction

Hydrogen isotope studies have for decades been used in a number of research fields such as hydrology [1], glacier studies [2–5], atmospheric and climate research [6,7]. The hydrogen and oxygen isotope composition of water samples have been used extensively in ice cores studies [3–5,8–10]. Traditionally the two principal approaches of obtaining hydrogen gas for stable isotope ratio analysis are the reduction method using metals (e.g., Cr, Mn, Ni, Zn and U) and the equilibrium techniques between water and hydrogen gas. Both techniques have been used for off-line and (semi) automated sample preparation methods [11–29]. Samples obtained by off-line hydrogen preparation are analysed by the classical dual inlet method, whereas for automatically prepared samples the dual inlet or the continuous flow (CF) methods are used in connection with an autosampler. With the CF method the samples are converted to gaseous hydrogen which is carried by a carrier gas (commonly helium) from the preparation system to the stable isotope ratio mass spectrometer (IRMS) [e.g., [30,31]]. Recently LASER spectroscopy of water samples has also been reported [32–34].

The equilibrium technique requires high stability control of the equilibrium temperature and furthermore involves corrections due to the fractionation occurring in the exchange reaction between water bound and gaseous hydrogen. An advantage of the metal reduction methods for preparation of sample gas for hydrogen isotope ratio analysis is the small sample size of <1 μl [25,28]. In contrast the equilibrium method requires 1–5 ml sample water [8,35,36].

Memory effects, i.e., reminiscences of the previous samples contaminate the sample being measured, are almost intrinsic to the metal reduction technique [11–18]. However, some instances of the Ni and Cr reduction methods are reported to be absent of memory effects [19–23]. In contrast memory effects of the equilibrium technique are rarely reported [35–37], although Huber and Leuenberger [10] reports of memory effects of 2% for an equilibrium system.

The origins of the memory effect may derive from multiple causes within the sample preparation system. Water is very susceptible to adsorption onto the inner surfaces of the glassware, stainless steal and chemicals of the inlet system; a property believed to lead to memory effects [10,28,38,39]. The

* Corresponding author. Tel.: +45 89423722.
E-mail address: jespero@phys.au.dk (J. Olsen).

1387-3806/$ – see front matter © 2006 Elsevier B.V. All rights reserved.
doi:10.1016/j.ijms.2006.05.004

memory effect may be caused by the downward movement of the oxidised to reducing front in the reactor as the chemicals are exhausted and may also be a function of the helium carrier flow or be dependent on reactant batch [13–16,40]. The syringe may carry reminiscences of previous samples causing memory effects which may be avoided by cleaning between subsequent injections using methanol or acetone wash solvents [14,27,38,41,42]. Syringe cleaning procedure can also be supplemented or replaced by flushing the syringe using samples as a wash agent [14,40,42]. Clearly if present, memory effects are limiting the accuracy and precision of the hydrogen isotope ratio analysis, and commonly the problems of memory effects can be minimised by avoiding large steps in hydrogen isotope composition in between samples, by replicate analysis or by applying corrections [15,16,33,40,42].

At the Aarhus AMS ^{14}C Dating Centre more than 14,000 ice core samples from the DYE-3, GRIP and NGRIP ice cores have been analysed [3,4] employing the chromium reduction continuous flow technique coupled to a GV-Instruments IsoPrime continuous flow isotope ratio mass spectrometry (CF-IRMS). The laboratory analyses water samples with a size of ~0.4 μl at a rate of 200 samples per day with a δD precision of 0.3–0.5‰. The relative abundance of ^{18}O to ^{16}O and ^{2}H to ^{1}H in ice cores can be used for counting annual accumulative layers, as fractionation depends on temperature and it is thus possible to differentiate between successive summers and winters [3,4,7,43–47]. However, counting annual layers using stable isotopes from ice cores is a very complex procedure, because the water molecules do not stay at fixed positions but diffuse, hence the yearly isotope signal is considerably smeared [46–51]. The establishment of an ice core chronology by using δD isotope signals from ice cores demands high precision measurements especially when analysing ice core samples from great depths. Therefore, it is of particular importance to reduce the memory effects observed in our system to a minimum. Furthermore, in order to manage the large amount of samples the objective has been to measure each ice core sample only once. Thus, the aim of this study has been to locate and quantify the causes of memory effects in our system in order to reduce them to a minimum, to perform a time optimisation of the analysis procedure and to develop correction procedures. Presented here is a systematic investigation of the influence of the syringe, injection port, gas chromatographic (GC) column and total analysis time on the magnitude of the memory effect. Further a correction algorithm is developed and tested.

2. Experimental

The deuterium measurements were produced with a Euro Vector elemental analyser (EA; EuroPyrOH-3100) combined with a Euro Vector liquid autosampler (LAS; EuroAS-300) and coupled to a GV-Instruments IsoPrime IRMS. The experimental setup is shown in Fig. 1. A syringe (SGE syringe 1 μl) fitted to the liquid autosampler pulls up ~0.4 μl of water from septum-sealed sample vials (2 ml) positioned in an autosampler with 110 storage points. The water sample enters the EA by the heated injector port held at 160 °C. At delivery the syringe penetrates a septum which seals the injector from atmosphere to a depth of 40 mm where it waits 1 s (pre dwell time) before injecting the water sample and then wait 2 s (post dwell time) before withdrawing again. Prior to the sample injection the syringe is washed with sample water one to five times. In each wash cycle 0.6 μl of water is taken up and injected into a waste vial. Then 0.4 μl of sample water is taken up for analysis together with 0.1 μl of air. After the injection the sample follows the helium flow through a tubular stainless steal liner which is a part of the injection port that extends into the quartz furnace (EuroVector, modified quartz reactor 18 mm/6 mm). In the furnace (1050 °C) the evaporated water sample is reduced by chromium (Goodfellow, 200 μm Chromium powder) to gaseous hydrogen molecules [15,28].

The hydrogen molecules are then transported through the GC column (160 °C) (EuroVector, 1.5 m 5 Å molecular sieve packed column) and further through an open split to the mass spectrometer. The sample gas entering the mass spectrometer generates simultaneous peaks of H_2 at the m/z 2 and HD m/z 3

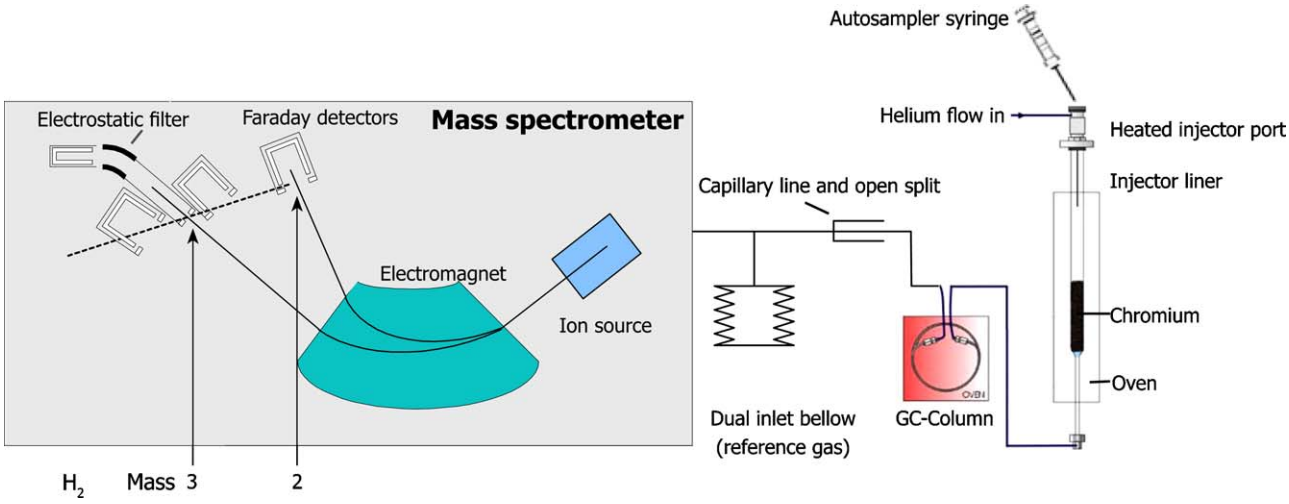

Fig. 1. Schematic layout of the experimental setup of the CF-IRMS system.

collectors. The m/z 3 collector is fitted with an electrostatic filter to avoid interference from helium tail flanks [28,52,53].

The measured isotope values are expressed using the conventional δD notation and converted to the VSMOW/SLAP scale [15,54–56] by first applying a drift correction to the raw δD values (i.e., measured δD values relative to machine reference gas) [10,15,16]. Calculation of the memory effect coefficients and optionally a correction for the memory effect may then be applied (see below).

3. Theory

The memory effect in the CF-IRMS system displaces the measured δD value of a sample x (δD_x) from the its true δD value ($\delta D_{x,\mathrm{True}}$). Hence, the true $\delta D_{x,\mathrm{True}}$ value of sample x may be written as the measured δD_x value of sample x minus a displacement M_x yielding

$$\delta D_{x,\mathrm{True}} = \delta D_x - M_x. \tag{1}$$

The magnitude of the displacement term M_x is in general unknown but may be found by modelling the nature of the memory effect.

The $\delta D_{x,\mathrm{True}}$ value can be determined by replicate analysis of sample x until the reminiscence of the previous samples have completely decayed. The reminiscence or memory effect of the previous sample $x-1$ can then be estimated by calculating the displacement $M_{x,i}$ divided by the transitional T step between samples x and sample $x-1$ yielding the fractional memory coefficients ϕ_i.

$$\phi_i = \frac{\delta D_{x,\mathrm{True}} - \delta D_{x,i}}{\delta D_{x,\mathrm{True}} - \delta D_{x-1,\mathrm{True}}} = \frac{M_{x,i}}{T}, \tag{2}$$

where i denotes the replication number of sample x. Practically this is done by setting up a series with two different standards with different isotopic composition which are measured alternately. The memory effect can then be observed as the deviation M_i between the measured and the true value of the second standard, divided by the transition step T between the two standards. The first replicate ($i=1$) of sample x contains the largest part of the reminiscence of the previous sample and is denoted the first memory coefficient ϕ_1.

Empirically it was found that the memory coefficients ϕ_i are best described by a double exponential fit $f(i)$:

$$F(i) = A\mathrm{e}^{-Bi} + C\mathrm{e}^{-Di}. \tag{3}$$

The constants A to D are determined by fitting $f(i)$ to the fractional memory coefficients ϕ_i (Eq. (2)) by the method of least squares. The constants B and D reflect the decay rate of the memory effect.

The unknown displacement term M_x of Eq. (1) equals the sum of the fitted memory coefficients $f(i)$ multiplied by the intersample transition steps T^* containing the previous z intersample transitions in backwards order. Hence, z is the backwards range of the memory effect. Unfortunately the transition step size between sample $x-1$ and sample x ($T_{x-1\to x}$) is unknown because the true δD_x value of sample x is unknown. However, this can be solved by defining the transition T as the displacement $M_{i,x}$ plus a remainder $R_{i,x}$. Thus, in general the transition T in Eq. (2) can be also be expressed as: $T = M_{i,x} + R_{i,x}$. Thus, rewriting Eq. (1) yields the $\delta D_{x,\mathrm{True}}$ value of sample x to be

$$\begin{aligned}\delta D_{x,\mathrm{True}} &= \delta D_x + \sum_{i=1}^{z} f_i \times T_{x-i\to x-i+1} \\ &= \delta D_x + \frac{f_1}{1-f_1} R_{x-1\to x} + \sum_{i=2}^{z} f_i \times T_{x-i\to x-i+1}.\end{aligned} \tag{4}$$

The calculation of the remainder term $R_{x-1\to x}$ for sample x preludes that the true $\delta D_{x-1,\mathrm{True}}$ value of sample $x-1$ is known. Hence, the correction of the first sample implies that the true δD value of the previous sample must be estimated. Practically this is done by initially estimating the true $\delta D_{x-1,\mathrm{True}}$ value of sample $x-1$ by replicate measurements on a standard until the memory effect has decayed. For the forthcoming samples the true δD values becomes known as subsequent samples are corrected. Note that no assumption on the characteristics of the correction coefficients $f(i)$ has been made. Thus, the fractional memory coefficients ϕ_i (Eq. (2)) may be used as a substitute for $f(i)$ as would any other estimation of $f(i)$.

4. Results

The memory effect has been monitored for all routine analyses since August 2002 and in addition a systematic investigation of the nature of memory effect has been carried out. Only measurements with intersample transition steps greater than 110‰ and more than 18 replicate injections of each standard have been used in the monitoring effort. For all transitions the fractional memory coefficients ϕ_i have been calculated according to Eq. (2).

The memory effect data obtained during routine analysis falls into two separate groups, one having an average of the first memory coefficient ϕ_1 of $5.9 \pm 0.6\%$ (Group I), and one with an average of ϕ_1 that equals $1.5 \pm 0.5\%$ (Group II). The double exponential fits are shown as lines in Fig. 2, together with the average and the standard deviation of the fractional memory coefficients ϕ_i and the fit parameters for the data in each group. The same decay trend can be seen in both graphs, and is a composite of a fast and slow decay component ranging over many post injections. Four systematic test sequences have been set up to investigate the influence from single system parameters on the memory effect. For all tests, the transition step size was 2500‰, achieved by using enriched samples. The memory effect for different combinations of injection volume (0.1–0.5 μl) and number of wash cycles (1–5) was performed in Test 1 as shown in Table 1 and Fig. 3. Tests 2–4 (see Table 2) were all performed using the same injection parameters. Test 2 was carried out in order to asses the influence of the injection needle on the memory effect by using separate syringes for each sample. The data are presented in Fig. 4. Test 3 was set up to investigate if the GC-column temperature has any influence on the memory effect. The temperature was set to 40 °C, 120 °C and 180 °C as displayed in

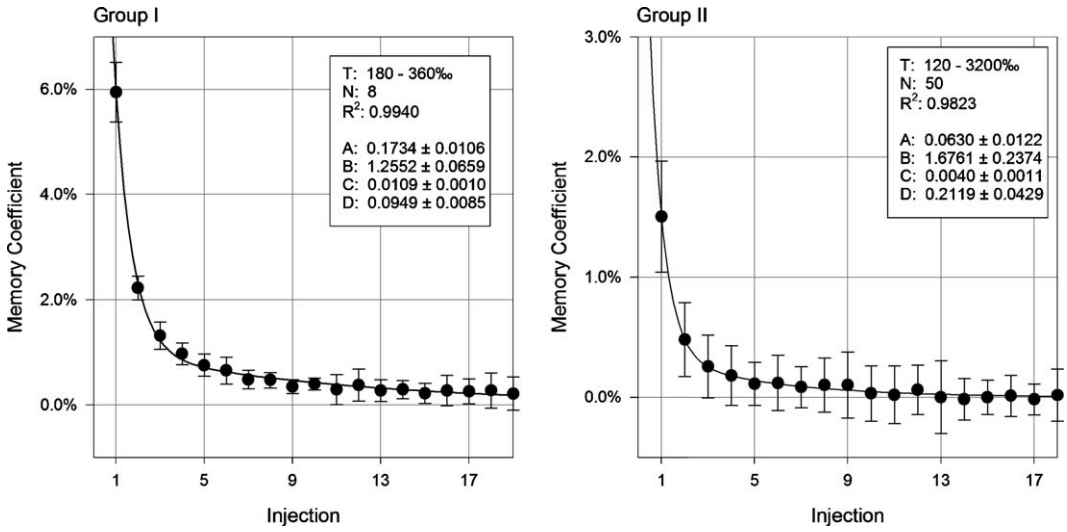

Fig. 2. The average and standard deviation memory coefficients ϕ_i obtained during routine analysis. The data falls in two groups; Groups I ($\phi_1 = 5.9 \pm 0.6\%$) and II ($\phi_1 = 1.5 \pm 0.5\%$). The solid lines represent the double exponential fits $f(i)$ to the memory coefficients ϕ_i.

Fig. 5. In Test 4 the influence of sample analysis time has been investigated.

The memory correction procedure has been examined by two tests. (1) A standard (Instaar GW1) has been interspersed in between ordinary samples at regular intervals and are denoted test Group B. The Instaar GW1 standard was also measured prior and post to test Group B and is denoted sequences A and C, respectively (see Table 3). (2) Seven standards has been setup in a sequence ranged after their isotopic composition in order to minimise the intersample transition step. Each standard was allowed to be measured only once, i.e., no replicate analysis (see Table 4), in order to simulate batch measurements of ordinary samples.

Table 1
Test of injection parameters

Test 1 method	Sample volume		Wash cycles
	ϕ_1 (%)	μl	
LAS-M1	4.36	0.1	1
LAS-M2	4.45	0.1	2
LAS-M3	3.79	0.1	3
LAS-M4	3.89	0.1	4
LAS-M5	2.61	0.1	5
LAS-M6	2.24	0.2	1
LAS-M7	2.67	0.2	2
LAS-M8	1.96	0.2	3
LAS-M9	2.61	0.2	4
LAS-M10	1.94	0.2	5
LAS-M11	1.95	0.3	1
LAS-M12	1.77	0.3	2
LAS-M13	1.74	0.3	3
LAS-M14	1.59	0.3	4
LAS-M15	1.80	0.3	5
LAS-M16	1.52	0.4	1
LAS-M17	1.47	0.4	2
LAS-M18	1.35	0.4	3
LAS-M19	1.45	0.4	4
LAS-M20	1.28	0.4	5
LAS-M21	1.41	0.5	1
LAS-M22	1.34	0.5	2
LAS-M23	1.25	0.5	3
LAS-M24	1.20	0.5	4
LAS-M25	1.15	0.5	5

All data obtained within 2 days using δD transitions above 2500‰, GC temperature at 160 °C, Thermogreen™ LB-2 septa and similar LAS injection configuration (air vol. 0.1 μl, fill vol. 0.6 μl, pro dwell 1 s, post dwell 2 s).

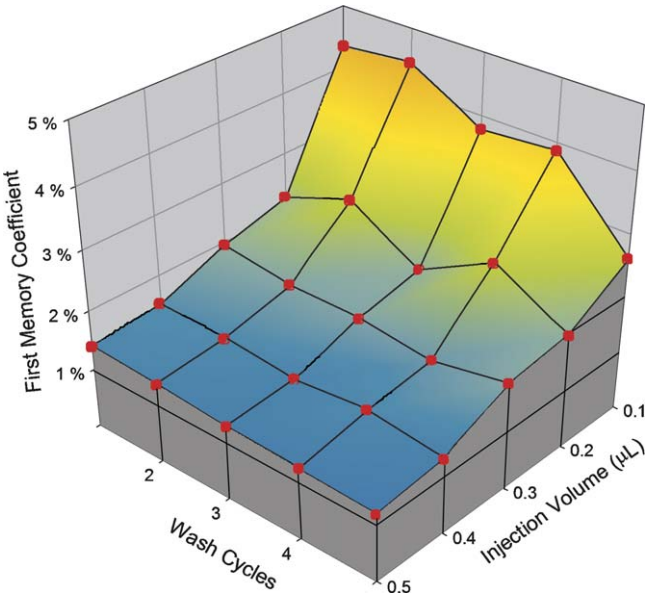

Fig. 3. Test 1: the first memory coefficient ϕ_1 plotted against the number of injection needle wash cycles and the injection volume. Note that for injection volumes >0.4 μl and for 1 or more wash cycles the memory effect is approximately constant.

5. Discussion

The most prominent reduction of the memory effect is observed from the bulk of routine data (Fig. 2). This reduction can be explained by replacement of the injection port liner to a type with greater length and larger diameter (Group I:

Table 2
Test of possible memory effect parameters

Total							
Test name	f_1	f_1 (slow)	Half range injections	f_1 (fast)	Half range injections	R^2	n
Test 2 (LAS injection needle)							
Pre washed needle	2.14%	0.355 ± 0.004%	2.3 ± 0.3	1.8 ± 0.8%	0.30 ± 0.02	1.000	4
Normal configuration	2.14%	0.503 ± 0.016%	2.1 ± 0.6	1.6 ± 0.8%	0.19 ± 0.12	0.991	3
Test 3 (GC-column temperature dependence)							
GC @40 °C	1.68%	0.446 ± 0.002%	2.5 ± 0.1	1.2 ± 0.3%	0.32 ± 0.01	1.000	2
GC@120 °C	1.86%	0.513 ± 0.004%	2.3 ± 0.2	1.3 ± 0.4%	0.36 ± 0.03	0.999	2
GC@180 °C	1.81%	0.466 ± 0.013%	1.6 ± 0.2	1.3 ± 0.6%	0.36 ± 0.04	0.999	2
Test 4 (analysis time length)							
Time @214 s	1.65%	0.513 ± 0.004%	2.5 ± 0.2	1.1 ± 0.9%	0.29 ± 0.04	0.998	3
Time @276 s	1.82%	0.592 ± 0.003%	3.1 ± 0.3	1.2 ± 2.4%	0.26 ± 0.05	0.997	3
Time @335 s	1.66%	0.420 ± 0.003%	3.0 ± 0.4	1.2 ± 1.3%	0.29 ± 0.05	0.997	6
Time @397 s	1.57%	0.367 ± 0.003%	3.1 ± 0.5	1.2 ± 0.9%	0.32 ± 0.05	0.996	3

All data obtained using δD transitions above 2500‰, GC temperature at 160 °C (except for Test 4), Thermogreen™ LB-2 septa and the similar LAS injection configuration (injection vol. 0.4 μl, wash cycles 3, see also note to Table 1). The coefficients f_1 and the half range given in injections are calculated from the least square fits of the data by Eq. (2).

Table 3
Test of the memory correction formula, Group I data

Batch	A: prior to samples	B: interspersed between samples		C: post to samples	Comparing test Group B with sequence (A + C)	
	Corrected δD (‰ VSMOW)	Uncorrected δD (‰ VSMOW)	Corrected δD (‰ VSMOW)	Corrected δD (‰ VSMOW)	Uncorrected (msd)	Corrected (msd)
GRIP1	−300.90 ± 0.33 (5)	−300.18 ± 0.36	−300.39 ± 0.28 (4)	−300.90 ± 0.23 (5)	0.52	0.26
GRIP2	−300.90 ± 0.49 (5)	−302.24 ± 1.24	−301.47 ± 0.43 (6)	−300.90 ± 0.45 (5)	1.80	0.33
GRIP3	−300.90 ± 0.64 (5)	−300.83 ± 0.25	−300.70 ± 0.32 (6)	−300.90 ± 0.53 (5)	0.00	0.04
GRIP4	−300.90 ± 0.37 (5)	−300.80 ± 0.77	−300.64 ± 0.84 (6)	−300.90 ± 0.55 (5)	0.01	0.07
GRIP5b	−300.90 ± 0.33 (5)	−299.33 ± 1.31	−299.95 ± 1.00 (3)	−300.90 ± 0.68 (5)	2.46	0.90
GRIP6	−300.90 ± 0.41 (5)	−300.00 ± 0.32	−300.93 ± 0.18 (5)	−300.90 ± 0.22 (5)	0.81	0.00
GRIP7	−300.90 ± 0.49 (5)	−300.34 ± 0.52	−301.42 ± 0.70 (6)	−300.90 ± 0.32 (5)	0.31	0.27
	−300.90 ± 0.17 (35)	−300.53 ± 0.30	−300.79 ± 0.23 (36)	−300.90 ± 0.17 (35)	0.85 ± 0.94	0.27 ± 0.31

msd: mean squared difference.

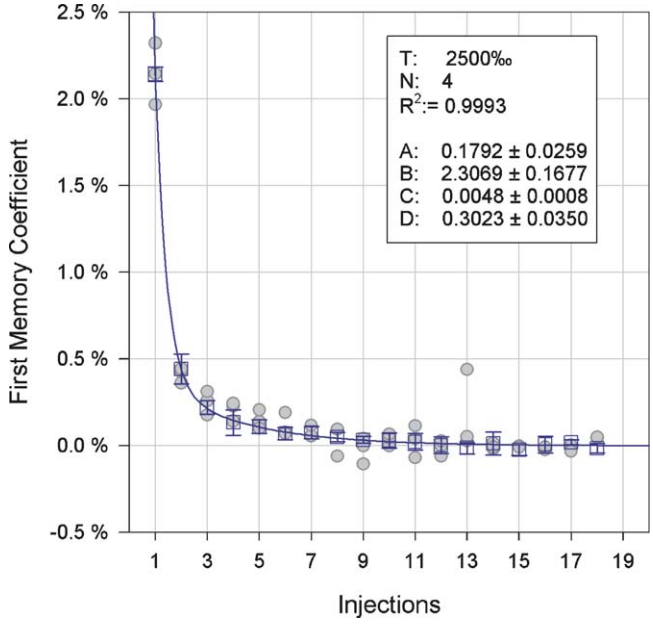

Fig. 4. Test 2: the memory effect of the injection syringe. Circular symbols: normal injection setup (see text). Squared symbols: a separate syringe has been used for each standard.

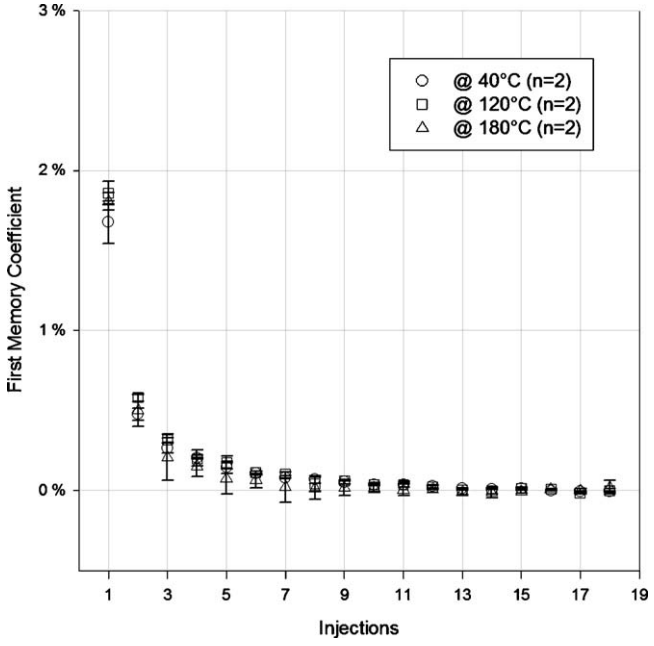

Fig. 5. Test 3: the memory effect dependence GC-column temperature.

Table 4
Test of the memory correction formula, Group II data

x	Sample	δD_{RAW} (‰)	T (‰)	$M_{1,x}$ (‰)	$\sum M_{2,x}$ to $M_{18,x}$ (‰)	$\delta D_{RAW\ (corrected)}$ (‰)	δD_{true} (‰ VSMOW)	$\delta D_{uncorrected}$ (‰ VSMOW)	msd	$\delta D_{corrected}$ (‰ VSMOW)	msd
1–18	SUMMIT	δD_{RAW}: −140.4 1.0‰ (n = 18, last five measurements used for estimating δD_{RAW})									
19	INSTAAR BW1	99.8	245.4	5.6	0.0	105.4	−123.3	−127.7	19.6	−123.2	0.0
20	KBH22	52.9	−52.2	−1.2	1.5	53.2	−168.8	−165.3	*	−165.1	*
21	INSTAAR WAIS	4.3	−49.4	−1.1	0.6	3.8	−204.5	−204.4	0.0	−204.8	0.1
22	CRETE	−64.0	−69.1	−1.6	0.3	−65.3	−261.6	−259.2	5.6	−260.3	1.8
23	INSTAAR GW1	−115.1	−51.1	−1.2	−0.2	−116.4	−300.9	−300.3	0.4	−301.3	0.2
24	GLACIAL	−277.3	−164.9	−3.7	−0.4	−281.4	−433.0	−430.5	6.1	−433.8	0.6
25	DOMEC	−290.9	−11.0	−0.2	−1.2	−292.3	−441.6	−441.5	0.0	−442.6	1.0
26	GLACIAL	−280.4	11.3	0.3	−0.9	−281.0	−433.0	−433.0	0.0	−433.5	0.2
27	INSTAAR GW1	−119.5	164.6	3.8	−0.6	−116.4	−300.9	−303.8	8.4	−301.3	0.1
28	CRETE	−68.7	49.2	1.1	0.5	−67.1	−261.6	−263.0	2.0	−261.7	0.0
29	INSTAAR WAIS	1.2	70.4	1.6	0.5	3.3	−204.5	−206.9	5.7	−205.2	0.5
30	KBH22	51.4	50.1	1.1	0.8	53.3	−168.8	−166.5	*	−165.0	*
31	INSTAAR BW1	103.7	52.4	1.2	0.9	105.8	−123.3	−124.5	1.6	−122.9	0.1
32	KBH22	52.8	−53.2	−1.2	1.0	52.5	−168.8	−165.4	*	−165.6	*
33	INSTAAR WAIS	3.4	−49.8	−1.1	0.4	2.7	−204.5	−205.1	0.3	−205.6	1.3
34	CRETE	−65.5	−69.7	−1.6	0.1	−67.1	−261.6	−260.5	1.3	−261.7	0.0
35	INSTAAR GW1	−115.2	−49.6	−1.1	−0.3	−116.6	−300.9	−300.3	0.3	−301.4	0.3
36	GLACIAL	−275.9	−163.5	−3.7	−0.5	−280.1	−433.0	−429.4	12.8	−432.7	0.1
37	DOMEC	−291.4	−12.9	−0.3	−1.4	−293.0	−441.6	−441.9	0.1	−443.1	2.3
38	GLACIAL	−279.7	12.6	0.3	−1.0	−280.4	−433.0	−432.5	0.3	−433.0	0.0
39	INSTAAR GW1	−118.6	164.9	3.8	−0.7	−115.5	−300.9	−303.1	4.6	−300.6	0.1
40	CRETE	−67.0	50.0	1.1	0.4	−65.5	−261.6	−261.7	0.0	−260.4	1.5
41	INSTAAR WAIS	2.5	70.0	1.6	0.5	4.5	−204.5	−205.9	1.8	−204.2	0.1
42	KBH22	53.0	50.4	1.1	0.8	54.9	−168.8	−165.3	*	−163.7	*
43	INSTAAR BW1	102.2	49.3	1.1	0.9	104.2	−123.3	−125.7	6.1	−124.1	0.8
44	KBH22	54.5	−49.9	−1.2	0.9	54.3	−168.8	−164.1	*	−164.2	*
45	INSTAAR WAIS	3.5	−51.5	−1.2	0.4	2.7	−204.5	−205.0	0.2	−205.6	1.2
46	CRETE	−64.1	−68.4	−1.6	0.0	−65.6	−261.6	−259.3	5.2	−260.5	1.2
47	INSTAAR GW1	−115.4	−51.2	−1.2	−0.3	−116.9	−300.9	−300.5	0.2	−301.7	0.6
48	GLACIAL	−277.0	−164.3	−3.7	−0.5	−281.2	−433.0	−430.3	7.3	−433.6	0.4
49	DOMEC	−291.4	−11.8	−0.2	−1.4	−293.0	−441.6	−441.9	0.1	−443.1	2.3
50	GLACIAL	−279.1	13.3	0.3	−1.0	−279.7	−433.0	−432.0	1.1	−432.4	0.3
51	INSTAAR GW1	−118.7	164.1	3.7	−0.7	−115.7	−300.9	−303.2	5.1	−300.7	0.0
52	CRETE	−66.2	51.0	1.2	0.4	−64.6	−261.6	−261.0	0.3	−259.7	3.6
53	INSTAAR WAIS	0.8	67.4	1.5	0.5	2.8	−204.5	−207.2	7.3	−205.6	1.2
54	KBH22	51.9	51.0	1.1	0.8	53.8	−168.8	−166.1	*	−164.6	*
55	INSTAAR BW1	103.4	51.6	1.2	0.9	105.4	−123.3	−124.8	2.4	−123.2	0.0
56	KBH22	54.3	−51.3	−1.2	1.0	54.1	−168.8	−164.2	*	−164.4	*
57	INSTAAR WAIS	4.7	−50.2	−1.1	0.4	3.9	−204.5	−204.0	0.2	−204.6	0.0
58	CRETE	−63.9	−69.4	−1.6	0.0	−65.5	−261.6	−259.2	5.9	−260.4	1.5
59	INSTAAR GW1	−115.7	−51.8	−1.2	−0.3	−117.2	−300.9	−300.8	0.0	−302.0	1.1
60	GLACIAL	−276.1	−163.1	−3.7	−0.5	−280.3	−433.0	−429.6	11.8	−432.9	0.0
61	DOMEC	−290.9	−12.2	−0.2	−1.4	−292.5	−441.6	−441.5	0.0	−442.7	1.3
62	GLACIAL	−278.8	13.1	0.3	−1.0	−279.5	−433.0	−431.8	1.5	−432.2	0.6
63	INSTAAR GW1	−119.2	163.3	3.7	−0.7	−116.2	−300.9	−303.6	7.2	−301.1	0.0
64	CRETE	−68.2	49.6	1.1	0.4	−66.6	−261.6	−262.6	0.9	−261.3	0.1
65	INSTAAR WAIS	2.3	71.0	1.6	0.5	4.4	−204.5	−206.0	2.1	−204.3	0.1
66	KBH22	52.4	49.9	1.1	0.8	54.3	−168.8	−165.7	*	−164.2	*
67	INSTAAR BW1	106.1	53.9	1.2	0.9	108.2	−123.3	−122.6	0.5	−120.9	5.5
									3.3 ± 4.3		0.9 ± 1.1

msd: mean squared difference.
* All δD values of the standard KBH 22 are enriched compared to the consensus δD value indicating that the bottle from which this standard was taken is leaking. Thus, the standard KBH 22 is not considered in the analysis.

L = 69 mm, i.d. = 2.1 mm; Group II: L = 99 mm, i.d. = 3.2). The strong influence of the injection port geometry on the memory effect can be due to its high ability to adsorb water vapour as it is made of stainless steal. A wider and longer liner increases the volume to surface ratio such that the adsorption probability for water molecules is much smaller as suggested by Morse et al. [38].

Empirically it has been found that the memory coefficient data (Groups I and II, Fig. 2) from the bulk analysis are well described by a double exponential decay function [26,42].

Thus, despite the reduced magnitude of memory effect between Groups I and II, the long range of the memory effect remains similar. A prolonged decay of the memory effect has also been reported elsewhere [16,40,57]. It may indicate that the memory effect originates from two different sources. Furthermore, these observations taken together indicate that a constant amount of water or hydrogen gas is adsorbed on the surface of the inlet system [38].

Within Group II the memory effect shows minor variations, ranging from 1% to 2.5%. The causes of the observed variations are difficult to pinpoint as often more than one system parameter is changed at the same time. Several authors have noted that the reactants and the packing of reactants in the reactor tube may cause significant memory effects [14,15,57,58]. Initially a mixing ratio of chromium and quartz chips of 4 to 1 with bottom filling of quartz chips was applied for routine analysis. The reactant replenishment rate and durability of this reactor packing was observed to be greatly varying in contrast to the findings by Itai and Kusakabe [58]. Therefore, by the method of trial and error other chemical packing configurations were explored. The best configuration seems to be of a reactor tube void of the bottom dead volume and using a chemical packing of pure chromium powder without any quartz chips. This reactor packing of pure chromium powder has been found to last more than 2000 injections. Similar findings have been reported by Nelson and Dettman [15]. However, they experimented on mixing different mesh sizes of chromium in order to increase the total reactive surface of chromium in the reactor. Further they observed that the first injections were reliable to display considerable scatter followed by excellent reproducibility; an experience also found on this system. Different types of injection port septa was tried out (Supelco, Hamilton Red Disc Septa (10 mm), Supelco, Thermogreen^{TM} LB-2 (11 mm) and Agilent, Low-Bleed Gray Septa (11 mm)) during routine analysis. The Hamilton Red Disc septum was susceptible of bleeding whereas no difference between the Thermogreen^{TM} LB-2 and Low-Bleed Gray Septa could be observed. The septa have in many instances been found to endure the life time of reactant chemicals, i.e., more than 2000 injections. Even though the data obtained during routine analysis are somewhat inconclusive, none of the described changes to the inlet system configuration could be correlated to significant changes in the memory effect.

Test 1, which is shown in Fig. 3 and Table 1 clearly show that there is a negative correlation between the memory effect and the sample size: the greater the sample volume, the lower the memory effect. In general a higher number of washes reduces the memory effect at a given sample volume. However, the number of syringe wash cycles has a less pronounced impact on the memory effect. Test 1 suggests that a sample volume of $\geq$0.4 μl and $\geq$1 wash cycles is the optimum combination balancing a low memory effect with a high degree of measuring efficiency. Thus, the number of syringe wash cycles can be significantly reduced compared to other reports [14,15,40,58] and the usage of wash solvents such as acetone or methanol can be totally avoided [14,27,41,42]. Furthermore, the adoption of only 1 wash cycle reduces the sample analysis time by about 20 s.

Using two separate syringes, one for each measured standard, the memory coefficients were determined according to Eq. (2), and compared to the memory coefficients determined employing one syringe and 3 wash cycles (Test 2, Fig. 4). As seen from Table 2 the first memory coefficient ϕ_1 determined by either method are equal. Hence, the syringe contributes by a negligible amount to the total memory effect for this configuration.

Test 3 and Fig. 5 indicate that the GC-column temperature has no impact on the memory effect, or at least, that it clearly appears to be a minor factor. At first this may seem as a surprising result as GC-columns are liable to have memory effects as they are adsorbing/desorbing the gaseous molecules (see, for example, [25,59]). Therefore, increasing the temperature of the GC-column should be expected to result in a decrease in the time interval between adsorption and desorbtion and thereby decrease the memory effect. However, the GC-column used for CF-EA hydrogen analysis is a molecular sieve GC-column. Thus, in principle only scattering with molecular sieve particles should occur and this should not result in intersample memory effects.

Reducing the analysis time is of great importance to total sample throughput. On the other hand, increasing the analysis times may be expected to reduce the memory effect as the system cleaning time between subsequent samples is prolonged due to the constant helium flow. Therefore, the contribution of total analysis time has been investigated. As can be seen from Test 4 (Table 2) the memory effect is not significantly influenced by the analysis time. Hence, the total analysis time is only restricted by the H_2 peak tailing.

It is an implicit assumption that the memory coefficient ϕ_i are independent of the intersample transition step size in order for the correction formula (4) to work properly. As observed from Fig. 6 the intersample transition step size and the first memory coefficients ϕ_1 are uncorrelated. In Table 3 (Group I data) the memory correction formula is evaluated against the mean square difference (msd) of the weighted average of the Instaar GW1 measurement prior (A) and post (C) of the samples of the interspersed test Group B. Similar Table 4 (Group II data) displays the mean square difference between the uncorrected and

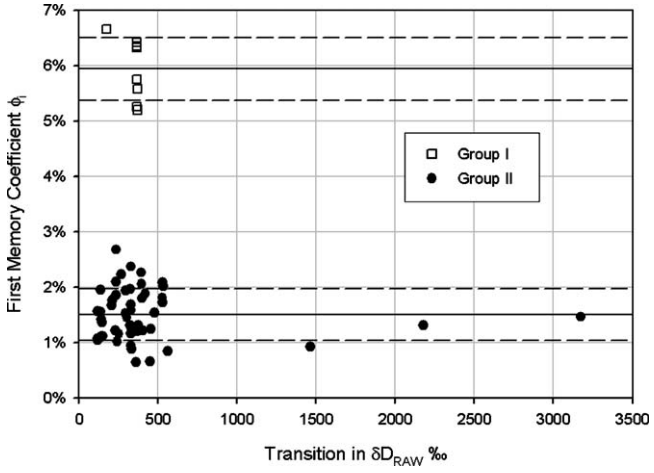

Fig. 6. The first memory coefficient ϕ_1 is displayed as a function of the transition step size T. The horizontal lines show the average value and the uncertainty of the first memory effect coefficients of Groups I and II.

corrected standards versus their true (consensus) δD value. In both cases the accuracy of the corrected δD values are improved significantly.

6. Conclusion

Memory effects are inherent to hydrogen isotope measurements in CF-IRMS systems. The system presented here employs the chromium reduction technique, and the memory effect has been investigated in order to optimise the system configuration for both minimal memory effects and time efficient δD measurements. The most prominent reduction of the inter-sample memory effect was achieved by the replacement of the injection port liner resulting in a reduction from 6% to 1–2%.

It may also be concluded that for small samples a few wash cycles strongly reduces the memory effect of the syringe for very small injection volumes. It has been shown that the most optimal combination for low memory effect and short analysis time is the injection of 0.4 μl of water sample with 1 wash cycle. Thus, sophisticated wash methods may be avoided. Further tests showed that the GC column temperature and the total analysis time did not have a significant impact on the magnitude of the memory effect. Hence, total analysis time is found to be limited only by H_2 tailing.

Empirically the memory effect has been found to be well described by a double exponential decay function. For a given system configuration the memory effect is of constant range and magnitude. A correction algorithm has been developed designed to take into account the long range of the memory effect and is found to significantly improve the accuracy of the δD measurements.

References

[1] N.O. Jorgensen, B.K. Banoeng-Yakubo, Hydro. J. 9 (2) (2001) 190.
[2] J.C. Yde, N.T. Knudsen, N.K. Larsen, C. Kornborg, O. Bjørslev-Nielsen, J. Heinemeier, J. Olsen, Ann. Gla. (2004) 42.
[3] I.K. Seierstad, S.J. Johnsen, B.M. Vinther, J. Olsen, Ann. Gla., 42, in press.
[4] B.M. Vinther, H.B. Clausen, S.J. Johnsen, S.O. Rasmussen, K.K. Andersen, S.L. Buchardt, I.K. Seierstad, M.-L. Siggaard-Andersen, J.P. Steffensen, A.M. Svenson, J. Olsen, J. Heinemeier, J. Geophys. Res., in press, doi:10.1029.2004JD006921.
[5] B.M. Vinther, S. Johnsen, K.K. Andersen, H.B. Clausen, A.W. Hansen, Geophys. Res. Lett. 30 (7) (2003) 1.
[6] T.S. Rhee, J. Mak, T. Röckmann, A.M. Brenninkmeijer, Rapid Commun. Mass Spectrom. 18 (2004) 299.
[7] W. Dansgaard, Tellas 16/4 (1964) 436.
[8] C. Huber, M. Leuenberger, Isotopes Environ. Health Stud. 41 (3) (2005) 189.
[9] S.J. Johnsen, D. DahlJensen, N. Gundestrup, J.P. Steffensen, H.B. Clausen, H. Miller, V. Masson-Delmotte, A.E. Sveinbjornsdottir, J. White, J. Qual. Sci. 16 (4) (2001) 299.
[10] C. Huber, M. Leuenberger, Rapid Commun. Mass Spectrom. 17 (12) (2003) 1319.
[11] C. Kendall, T.B. Coplen, Anal. Chem. 57 (1985) 1437.
[12] R.A. Socki, C.S. Romanek, E.K. Gibson, Anal. Chem. 71 (11) (1999) 2250.
[13] I.S. Begley, C.M. Scrimgeour, Rapid Commun. Mass Spectrom. 10 (1996) 969.
[14] T. Donnelly, S. Waldron, A. Tait, J. Dougans, S. Bearhop, Rapid Commun. Mass Spectrom. 15 (15) (2001) 1297.
[15] S.T. Nelson, D. Dettman, Rapid Commun. Mass Spectrom. 15 (23) (2001) 2301.
[16] B.H. Vaughn, J.W.C. White, M. Delmotte, M. Trolier, O. Cattani, M. Stievenard, Chem. Geol. 152 (1998) 309.
[17] H.J. Tobias, K.J. Goodman, C.E. Blacken, J.T. Brenna, Anal. Chem. 67 (1995) 2486.
[18] M. Gehre, New Approaches for Stable Isotope Ratio Measurements, Vienna, IAEA-TECDOC-1247, 1999.
[19] S.D. Kelly, K.D. Heaton, P. Brereton, Rapid Commun. Mass Spectrom. 15 (15) (2001) 1283.
[20] W.A. Brand, H. Avak, R. Seedorf, D. Hofmann, T. Conradi, Isotopes Environ. Health Stud. 32 (1996) 263.
[21] M. Gehre, R. Hoefling, P. Kowski, G. Strauch, Anal. Chem. 68 (1996) 4414.
[22] H.J. Tobias, J.T. Brenna, Anal. Chem. 68 (1996) 2281.
[23] S.D. Kelly, I.G. Parker, M. Sharman, M.J. Dennis, J. Mass Spectrom. 33 (1998) 735.
[24] J. Bigelsen, M.L. Perlman, H.C. Prosser, Anal. Chem. 24 (1952) 1356.
[25] Z.D. Sharp, V. Atudorei, T. Durakiewicz, Chem. Geol. 178 (2001) 197.
[26] W.W. Wong, M.P. Cabrera, P.D. Klein, Anal. Chem. 56 (1984) 1852.
[27] S. Ward, M. Scantlebury, E. Król, P.J. Thomson, C. Sparling, J.R. Speakman, Rapid Commun. Mass Spectrom. 14 (2000) 450.
[28] J. Morrison, T. Brockwell, T. Merren, F. Fourel, A.M. Phillips, Anal. Chem. 73 (15) (2001) 3570.
[29] I. Friedman, Geochim. Cosmochim. Acta 4 (1953) 89.
[30] A.J. Midwood, B.A. McGaw, Anal. Commun. 36 (1999) 291.
[31] J.T. Brenna, T.N. Corso, H.J. Tobias, R.J. Caimi, Mass Spectrom. Rev. 16 (1997) 227.
[32] R. van Trigt, Wiskunde en Natuurwettenschappen, Rijksuniversiteit Groningen, Groningen, 2002.
[33] R. van Trigt, E.R.T. Kerstel, G.H. Visser, H.A.J. Meijer, Anal. Chem. 73 (11) (2001) 2445.
[34] E.R.T. Kerstel, V.R. Trigt, H.A.J. Meijer, G.H. Visser, S. Johnsen, Proceedings of the 1st International Symposium on Isotopomers, Yokohama, Japan, 2001.
[35] F. Thielecke, W. Brand, R. Noack, J. Mass Spectrom. 33 (4) (1998) 342.
[36] H. Meyer, L. Schönicke, U. Wand, H.W. Hubberten, H. Friedrichsen, Isotopes Environ. Health Stud. 36 (2000) 133.
[37] S.J. Prosser, C.M. Scrimgeour, Anal. Chem. 67 (1995) 1992.
[38] A.D. Morse, I.P. Wright, C.T. Pillinger, Chem. Geol. 107 (1–2) (1993) 147.
[39] J.M. Eiler, N. Kitchen, Geochim. Cosmochim. Acta 65 (2001) 4467.
[40] M. Gehre, H. Geilmann, J. Richter, R.A. Werner, W.A. Brand, Rapid Commun. Mass Spectrom. 18 (2004) 2650.
[41] I.S. Begley, C.M. Scrimgeour, Anal. Chem. 69 (1997) 1530.
[42] P. Franz, Röckmann, Rapid Commun. Mass Spectrom. 18 (2004) 1429.
[43] S. Epstein, R.P. Sharp, Trans. Am. Geophys. Union 1 (1959) 81.
[44] B. Benson, Stratigraphic studies in the snow and firn of the Greenland ice sheet, U.S. Snow, Ice and Permafrost Research Establishment, Research Report, 1962, p. 70.
[45] C.U. Hammer, H.B. Clausen, W. Dansgaard, N. Gundestrup, S.J. Johnsen, N. Reeh, J. Glaciol. 20 (82) (1978) 3.
[46] S. Johnsen, H.B. Clausen, J. Jouzel, J. Schwander, A.E. Sveinbjörndöttir, J. White, in: J.S. Wettlaufer, J.G. Dash, N. Untersteiner (Eds.), Ice Physics and the Natural Environment, Springer–Verlag, Berlin Heidelberg, 1999.
[47] W. Dansgaard, S.J. Johnsen, H.B. Clausen, N. Gundestrup, Meddelelser om Grønland 197 (2) (1973) 1.
[48] C.C. Langway Jr., Stratigraphic analysis of a deep ice core from Greenland, Cold Regions Research and Engineering Laboratory, Research Report, 1967, p. 1.
[49] S.J. Johnsen, Proceedings of the Grenoble Symposium on Isotopes and Impurities in Snow and Ice, Grenoble, Aug./Sep. 1975, IAHS Publ., 1977, p. 210.

[50] S. Johnsen, H.B. Clausen, K.M. Cuffey, G. Hoffmann, J. Schwander, T. Creyts, in: T. Hondoh (Ed.), Physics of Ice Core Records, Hokkaido University Press, Sapporo, 2000, p. 121.
[51] J. Southon, Radiocarbon 46 (3) (2004) 1239.
[52] A.W. Hilkert, C.B. Douthitt, H.J. Schluter, W.A. Brand, Rapid Commun. Mass Spectrom. 13 (13) (1999) 1226.
[53] T. Merren, Application of an Electrostatic Filter for the Measurement of Hydrogen Isotopes in Continuous Flow Mode IRMS, Micromass UK, Manchester, 2000.
[54] T.B. Coplen, Chem. Geol. 72 (1988) 293.
[55] T.B. Coplen, J. Res. Natl. Inst. Stand. Technol. 100 (3) (1996) 285.
[56] T.B. Coplen, Guidelines for the Reporting of Stable Hydrogen, Carbon, and Oxygen Isotope-Ratio Data, http://wwwrcamnl.wr.usgs.gov/isoig/res/guide.html, 2004.
[57] G.D. Farguhar, B.K. Hemry, J.M. Styles, Rapid Commun. Mass Spectrom. 11 (1997) 1554.
[58] K. Itai, M. Kusakabe, Geochem. J. 38 (2004) 435.
[59] A.T. Aerts-Bijma, J. van der Plicht, H.A.J. Meijer, Radiocarbon 43 (2001) 293.